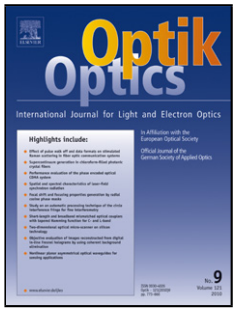


Title: Determination of Beam Incidence Conditions Based on the Analysis of Laser Interference Patterns

Author: Dapeng Wang Zuobin Wang Yong Yue Juncai Yu Chunlei Tan Dayou Li Renxi Qiu Carsten Maple

PII: S0030-4026(15)00591-4
DOI: http://dx.doi.org/doi:10.1016/j.ijleo.2015.07.039
Reference: IJLEO 55754

To appear in:

Received date: 26-5-2014
Accepted date: 4-7-2015

Please cite this article as: D. Wang, Z. Wang, Y. Yue, J. Yu, C. Tan, D. Li, R. Qiu, C. Maple, Determination of Beam Incidence Conditions Based on the Analysis of Laser Interference Patterns, *Optik - International Journal for Light and Electron Optics* (2015), http://dx.doi.org/10.1016/j.ijleo.2015.07.039

# Determination of Beam Incidence Conditions Based on the Analysis of Laser Interference Patterns

**Dapeng Wang[a,b], Zuobin Wang[a,b], Yong Yue[a,b,c], Juncai Yu[a], Chunlei Tan[d], Dayou Li[b], Renxi Qiu[b], Carsten Maple[b]**

[a]Changchun University of Science and Technology, JR3CN & CNM, Changchun, China, 130022

[b]University of Bedfordshire, JR3CN & IRAC, Luton, UK, LU1 3JU

[c]Xi'an Jiaotong-Liverpool University, DCSSE, Suzhou, China, 215123

[d]Tampere University of Technology, ORC, Tampere, Finland, FIN-33101

**Abstract.** Beam incidence conditions in the formation of two-, three- and four-beam laser interference patterns are presented and studied in this paper. In a laser interference lithography (LIL) process, it is of importance to determine and control beam incidence conditions based on the analysis of laser interference patterns for system calibration as any slight change of incident angles or intensities of beams will introduce significant variations of periods and contrasts of interference patterns. In this work, interference patterns were captured by a He-Ne laser interference system under different incidence conditions, the pattern period measurement was achieved by cross-correlation with, and the pattern contrast was calculated by image processing. Subsequently, the incident angles and intensities of beams were determined based on the analysis of spatial distributions of interfering beams. As a consequence, the relationship between the beam incidence conditions and interference patterns is revealed. The proposed method is useful for the calibration of LIL processes and for reverse engineering applications.

**Keywords:** Laser interference, Beam incidence condition, Modulation period, Interference lithography.

**Address all correspondence to:** Zuobin Wang, Changchun University of Science and Technology, JR3CN & CNM, Changchun, China, 130022; Tel: +86 43185582341, Fax: +86 43185582925; E-mail: wangz@cust.edu.cn

## 1 Introduction

Laser interference lithography (LIL), as a powerful method for the fabrication of periodic micro and nano structures, is attracting extensive attentions for many applications [1, 2]. Besides the merits of high efficiency and low cost, LIL is developed to break through the limited area yielded by electron beam lithography (EBL) or focused ion beam lithography (FIBL) and fulfill the large-area fabrication. LIL is also a flexible method capable of producing various sub-wavelength fringe and dot structures in the cases of two-, three- and four-beam laser interference [3-8]. Recently, researchers reported that a wide variety of applications were achieved by LIL. Guo et al. employed two-beam laser interference technology to pattern graphene oxide and hierarchical nanostructures were formed for the

production of a high performance humidity sensing device [9]. Guo and his co-worker reported that large-area microlens arrays were fabricated via a single step by laser interference ablation [10]. Jin et al. used two-beam LIL to fabricate metallic electrodes and enhanced the absorption in organic solar cells [11]. Castro-Hurtado et al. reported that the tungsten oxide ($WO_3$) thin films were modified by three- and four-beam laser interference lithography and the nanostructures with the feature sizes of 150-160nm in diameter were achieved. In the conclusion, they pointed out that the outstanding nanostructured films could be used as sensing layers for the detection of hazardous gases such as $NO_2$ and $H_2S$ [12]. It can be seen from literatures that numerous efforts have been devoted to the fabrication of devices and functional materials based on the micro and nano structures by LIL. But, both theoretically and experimentally, the beam incidence conditions play a critical role in the determination of period and contrast in the formation of interference patterns.

It is known that the period of interference can be controlled by changing the incident angles of beams or the radiation wavelength [13]. For practical applications, the wavelength is first selected so that the period depends on the incident angles. Meanwhile, the influences of polarized angles, azimuth angles and number of beams are also extremely important for obtaining desired interference patterns since the spatial distributions of interfering beams are a function of the mentioned parameters. In the case of two-beam laser interference, different incidence conditions introduced by the polarization vectors result in different contrasts [14]. In the case of three-beam laser interference, the modulation period is produced in the coplanar incidence conditions, and in the case of four-beam interference, there are three different types of patterns produced by polarization modes [15]. To determine the relationship between the beam incidence conditions and interference patterns, a series of steps, including image acquisition, processing and analysis based on the theory of physical optics, were taken to achieve high precision measurement and offer an effective way for the calibration of LIL processes.

In the previous approaches, apart from direct measurement and Hough transform methods [16-18], mean-square-difference algorithm was employed to determine the period and slope of oblique fringes [19]. It was demonstrated that the methods had the advantages of averaging noise and nano-scale accuracy to measure two-beam interference patterns [20]. However, there has been no published work on three- and four-beam interference measurements to determine the beam incidence conditions**.**

In a LIL process, any slight change of incident angles or intensities of beams will introduce significant variations of periods and contrasts of interference patterns, thus, it is essential to determine and control beam incidence conditions based on the analysis of laser interference patterns for system calibration. In this work, a He-Ne laser interference system was set up to obtain various interference patterns configuring different beam incidence conditions. Cross-correlation was applied to the calculation of periods and the pattern contrast was calculated by extracting the maximum and minimum grey-scale values from selected image patches or regions and averaging every contrast value of the whole region. Two-beam incidence conditions, three-beam coplanar and non-coplanar incidence conditions and four-beam incidence conditions have been studied, and the calculations have been carried out systematically. The incident angles or intensities of beams are determined subsequently.

## 2 Fundamental Theories

### *2.1 Principle of LIL*

A general form of *N*-beam laser interference can be considered as the superposition of electric field vectors of *N* beams ( $\vec{E}_1, \vec{E}_2, \vec{E}_3$, ... and $\vec{E}_N$ ) and the *m*th vector can be written as

$$\vec{E}_m = A_m \vec{p}_m \cos(\vec{k}_m \cdot \vec{r}_m - \omega \cdot t + \delta_m). \quad (1)$$

In the electric field vector, $\vec{k}_m$ and $\vec{p}_m$ can be expressed by

$$\vec{k}_m = k(\sin\theta_m \cdot \cos\phi_m \cdot \vec{i} + \sin\theta_m \cdot \sin\phi_m \cdot \vec{j} - \cos\theta_m \cdot \vec{k}), \quad (2)$$

$$\begin{aligned}\vec{p}_m = &-(\cos\theta_m \cdot \cos\phi_m \cdot \cos\psi_m - \sin\phi_m \cdot \sin\psi_m)\vec{i} \\ &-(\cos\theta_m \cdot \sin\phi_m \cdot \cos\psi_m + \cos\phi_m \cdot \sin\psi_m)\vec{j}\,, \\ &-(\sin\theta_m \cdot \cos\psi_m)\vec{k}\end{aligned} \tag{3}$$

where $A_m$ is the amplitude, $\vec{p}_m$ is the unit polarization vector, $\vec{k}_m$ is the vector in the propagation direction, $\vec{r}_m$ is the position vector, $\omega$ is the frequency, $\delta_m$ is the initial phase, $k = 2\pi/\lambda$, $\lambda$ is the wavelength, $\theta_m$ is the incident angle, $\phi_m$ is the azimuthal angle, and $\psi_m$ is the polarized angle.

In the interference area, the intensity distribution can be expressed as

$$I(r) = \left|\sum_{m=1}^{N} \vec{E}_m\right|^2 = \sum_{m=1}^{N}\sum_{n=1}^{N} A_m \vec{p}_m \cdot A_n \vec{p}_n \cdot e^{[i(\vec{k}_m - \vec{k}_n)\vec{r} + \delta_m - \delta_n]}. \tag{4}$$

It has been demonstrated that the polarization vector plays a key role in the formation of interference patterns [14]. Thus, two-, three- and four-beam laser interference formulas with proposed beam incidence conditions are derived from Eqs. (1)-(4), which are discussed in the following sections.

*2.2 Image processing algorithms*

In order to determine the period of the interference patterns, two patches of interference patterns are selected as the fixed and reference image patches. It can be calculated that the fixed patch matches with the reference patch by means of the cross-correlation coefficient which represents the similarity numerically. The schematic of this algorithm is shown in Fig. 1(a). The correlation coefficient, $\rho_{XY}$, between two matrices from the two image patches *X* and *Y* is defined as:

$$\rho_{XY} = \frac{\mathrm{cov}(X,Y)}{\sigma_X \sigma_Y} = \frac{E[(X - \mu_X)(Y - \mu_Y)]}{\sigma_X \sigma_Y}. \tag{5}$$

where *E* is the expected value, cov is the covariance, $\mu_X$ and $\mu_Y$ are the mean values of X and Y, and $\sigma_X$ and $\sigma_Y$ are the standard deviations.

According to the theory of optics, the interference contrast is defined as

$$K = \frac{I_{max} - I_{min}}{I_{max} + I_{min}}. \quad (6)$$

where $I_{max}$ and $I_{min}$ are the maximum and minimum interference intensities. For the calculation of contrast, the pattern is divided into N patches or regions. The pattern contrast can be calculated by extracting the maximum and minimum grey-scale values in every selected patches or regions firstly and then averaging the contrast values of the whole image. Fig. 1(b) illustrates the schematic of this algorithm.

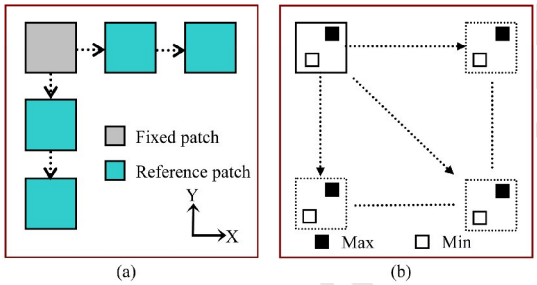


**Fig. 1** The schematic of image processing algorithms. (a) Principle of determining the period by pattern correlation; (b) Principle of determining the contrast.

## 3 Experimental Details

In the experiment, the He-Ne laser (CVI Melles Griot, 25-LHP-213) with the wavelength of 633nm and output power of 0.5mw was used for the LIL imaging system. The laser source takes advantages of good beam quality and 30cm coherent length. To perform real-time imaging, a CCD camera (PiontGrey, CMLN-13S2M-CS) replaces the exposed sample and a 20x Calilean beam expander is fixed before the camera as the period of interference is far smaller than the CCD pixel size.

The scheme of four different experimental setups is shown in Fig. 2. The main laser beam was divided into two, three or four coherent beams by beamsplitters and high-reflective mirrors. Half-wave plates and polarizers were used to control the power and polarized angles precisely.

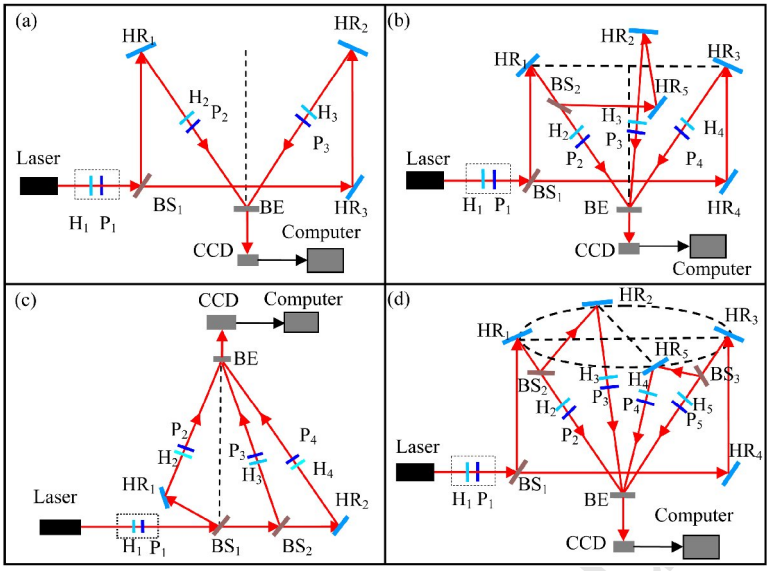


**Fig. 2** Schematic set-up for (a) Two-beam laser interference; (b) Non-coplanar three-beam laser interference; (c) Coplanar three-beam laser interference; (d) Four-beam laser interference. $HR_1$, $HR_2$, $HR_3$, $HR_4$, and $HR_5$ are the high-reflective mirrors, $BS_1$, $BS_2$ and $BS_3$ are the beamsplitters, $H_1$, $H_2$, $H_3$, $H_4$ and $H_5$ are the half wave plates, $P_1$, $P_2$, $P_3$, $P_4$ and $P_5$ are the polarizers and BE is the 20× Calilean beam expander.

## 4 Results and Discussions

### *4.1 Two-beam interference*

In the two-beam laser interference, a periodic fringe pattern is produced with the incident angles of $\theta_1 = \theta_2 = \theta$, the azimuthal angles of $\phi_1 = 0°$ and $\phi_2 = 180°$, and the polarized angles of $\psi_1 = \psi_2 = 90°$, the intensity distribution can be expressed by

$$I_{two-beam} = A_1^2 + A_2^2 - 2A_1A_2\cos[k\ (\sin\theta_1 + \sin\theta_2)x]. \quad (7)$$

It can be seen from Eq. (7) that the period of the interference pattern is $d=\lambda/2\sin\theta$ in the case of the symmetrical two-beam incidence. Fig. 3(a) is the fringe pattern obtained by the CCD camera. The pixel number of phase shifts is 29.577 in Fig. 3(b). The pixel size of the CCD is 3.75μm, and the measured period of the interference pattern is 5.546μm. In the experiments, the incident angles were set as $\theta_1 = \theta_2 = 3.3°$, which resulted in the period of 5.498μm theoretically. It is found that the offset between the designed angles and the measured angles is 0.03°. Moreover, with the calculation of the contrast, the intensity of each beam can be

determined. The maximum and minimum grey-scale values are extracted from the 96×128 pixels patches which shift in the whole interference pattern. The final value is obtained by averaging all the contrasts with the shifting step of 10 pixels from the row and column directions. According to Eqs. (6) and (7), in this case, $K$ can be written as

$$K_{two-beam} = \frac{2A_1A_2}{A_1^2 + A_2^2}, \tag{8}$$

and the calculation result is 0.87. It can be concluded that the amplitude of one beam is 1.7 times higher than that of the other one.

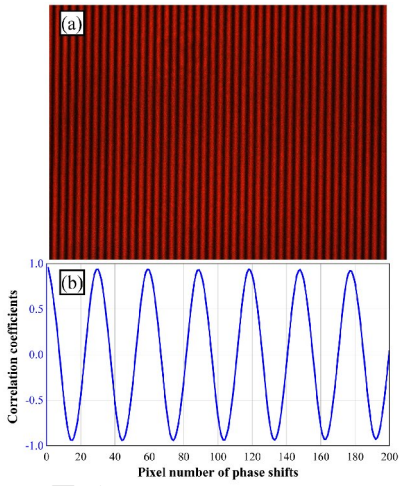


**Fig. 3** (a) The CCD image of the two-beam laser interference; (b) Corresponding correlation coefficients as a function of phase shifts.

*4.2 Three-beam interference in the non-coplanar incidence condition*

In the cases of three-beam laser interference, there are generally two different configurations corresponding to coplanar and non-coplanar incidence conditions. The triangle distribution pattern is generated by the non-coplanar incidence condition while the dual-grating pattern is generated by the coplanar incidence condition, as shown in Fig. 4. In the non-coplanar incidence condition, the three beams have the same incident angles of $\theta_1 = \theta_2 = \theta_3 = \theta$, and the azimuthal angles of 30°, 150° and 270°. In the coplanar incidence

condition, the incident angles of three beams are $\theta_1 = \theta_2 = \theta$ , $\theta_3 = \theta^*$ ( $\theta^* > \theta$ ), and the azimuthal angles are, $\phi_1 = \phi_3 = 0°$ and $\phi_3 = 180°$ .

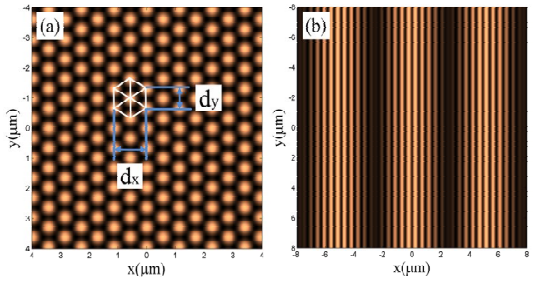


**Fig. 4** 2D simulations of three-beam interference distributions. (a) Non-coplanar incidence condition; (b) Coplanar incidence condition.

According to Eqs. (1)-(4), when the polarized angles are 0°, the equation of the three-beam interference in the non-coplanar incidence condition is expressed as

$$\begin{aligned} I_{three-beam} &= A_1^2 + A_2^2 + A_3^2 + \Delta \cdot A_1 A_2 \cos(k\sqrt{3}\sin\theta \cdot x) \\ &+ \Delta \cdot A_1 A_3 \cos(k\frac{\sqrt{3}}{2}\sin\theta \cdot x + k\frac{3}{2}\sin\theta \cdot y), \\ &+ \Delta \cdot A_2 A_3 \cos(k\frac{\sqrt{3}}{2}\sin\theta \cdot x - k\frac{3}{2}\sin\theta \cdot y) \end{aligned} \tag{9}$$

where $\Delta = 2\sin^2\theta - \cos^2\theta$ . It can be seen that the period in the x direction is

$$d_x = 2\lambda/\sqrt{3}\sin\theta, \tag{10}$$

and the period in the y direction is

$$d_y = 2\lambda/3\sin\theta. \tag{11}$$

This means that the period in the x direction is $\sqrt{3}$ times larger than the other one, which shows a good correspondence with the simulation in Fig. 4(a). Thus, the three-beam laser interference method is able to generate the triangle or hexagon distribution pattern.

The triangle pattern shown in Fig. 5(a) was obtained experimentally. Fig. 5(b) indicates that the respective pixel numbers of phase shifts in the x and y directions are unequal. According to the results of the correlation coefficient calculations, the measured period in the x direction is $d_x$=7.854μm and that in the y direction is $d_y$=4.401μm. The relationship of the

ideal pattern is $d_x/d_y=\sqrt{3}$ and the experimental relationship is $d_x/d_y=1.785$. It is demonstrated that the misalignment of the azimuthal angles causes a minor offset of 0.74° between the designed angles and the measured angles. Unlike the two-beam interference, the contrast of the three-beam interference in the non-coplanar incidence conditions is determined by the amplitude of each beam and has an effect on the incident angles. The contrast in this case is expressed as

$$K_{three-beam}=\Delta\cdot\frac{A_1A_2+A_1A_3+A_2A_3}{A_1^2+A_2^2+A_3^3}. \tag{12}$$

To calculate the contrast, the incident angle needs to be determined first. As Fig. 5(b) and Eq. (10) suggested, the incident angle is 5.3°, so $\Delta=0.9744$. Meanwhile, the contrast is calculated by the image processing method which is used in the two-beam interference and the result is 0.9706. Thus, it is demonstrated that the amplitudes are almost equal with each other.

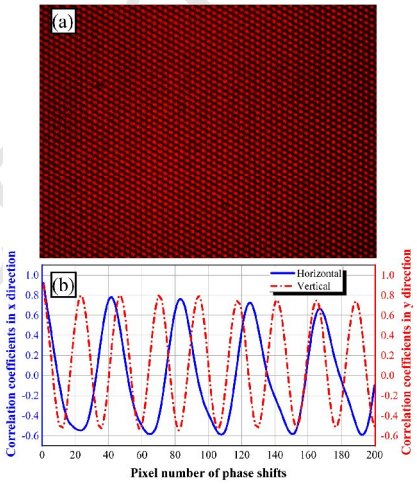


**Fig. 5** (a) The CCD image of the three-beam laser interference in the non-coplanar incidence condition; (b) Corresponding correlation coefficients in x and y directions as a function of phase shifts.

*4.3 Three-beam interference in the coplanar incidence condition*

When the azimuthal angles of three beams are in the same plane, a dual-grating structure pattern is produced. In the experiment, the initial laser beam was divided into three beams with the azimuthal angles of $\phi_1=\phi_3=0°$ and $\phi_2=90°$, the polarized angles of

$\psi_1 = \psi_2 = \psi_3 = 90°$, and the incident angles of $\theta_1 = \theta_2 = \theta$ and $\theta_3 = \theta^*$ ($\theta^* > \theta$). In this case, the intensity of interference $I'_{three-beam}$ is expressed as

$$\begin{aligned} I'_{three-beam} = {} & A_1^2 + A_2^2 + A_3^2 - 2A_1A_2\cos(2k\sin\theta \cdot x) \\ & + 2A_1A_3\cos[(\sin\theta - \sin\theta^*)x - (\cos\theta - \cos\theta^*)z] \\ & - 2A_2A_3\cos[(\sin\theta + \sin\theta^*)x + (\cos\theta - \cos\theta^*)z] \end{aligned} . \quad (13)$$

Eq. (13) indicates that the intensity of interference is a function of the coordinates in the x and z directions. Generally, the interference is deemed to occur in the xy plane. This means that the value of z is zero, so there are three interference terms in the x directions. They are expressed as

$$\begin{cases} d_1 = \dfrac{\lambda}{2\sin\theta} \\ d_2 = \dfrac{\lambda}{\sin\theta + \sin\theta^*} \\ d_3 = \dfrac{\lambda}{\left|\sin\theta - \sin\theta^*\right|} \end{cases} . \quad (14)$$

In practice, $\theta^*$ and $\theta$ are approximately equal with each other, consequently, $d_1$ and $d_2$ are approximately equal, and $d_3$ is larger than them ($d_1 \approx d_2$, $d_3 >> d_1$). Thus, it is the reason that the interference pattern exhibits dual periods. Fig. 6 shows the experimental result. From the curve in Fig. 6(b), the periods are calculated as $d_1$=3.5625μm, $d_2$=3.1875μm and $d_3$=27.5625μm. According to the values and Eq. (14), the incidence conditions can be determined, and they are $\theta = 5.1°$ and $\theta^* = 6.3° \pm 0.3°$.

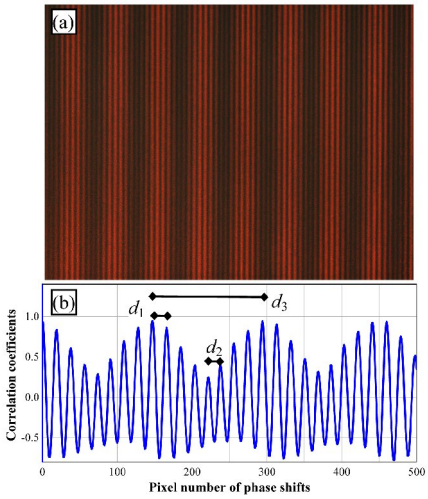


**Fig. 6** (a) The CCD image of the three-beam laser interference in the coplanar incidence condition; (b) Corresponding correlation coefficients as a function of phase shifts.

In this case, the contrast is expressed as

$$K'_{three-beam} = \frac{A_1A_2 + A_1A_3 + A_2A_3}{A_1^2 + A_2^2 + A_3^3}. \tag{15}$$

and the calculation result is 0.734. The decrease of contrast could be caused by the unequal amplitudes of each beam.

*4.4 Four-beam interference*

The four beams follow a symetrical configuration with the azimuthal angles of 0°, 90°, 180° and 270°. The polarization angles of four beams were 90°. It can be seen in Fig. 7(a) that a two-dimensional grating pattern and periodic dots are produced in this case and the maximum intensities distribute along both x and y axes. The formula of the four-beam laser interference can be expressed as

$$\begin{aligned} I_{four-beam} = {} & A_1^2 + A_2^2 + A_3^2 + A_4^2 - 2A_1A_3\cos[k\ (\sin\theta_1 + \sin\theta_3)x] \\ & - 2A_2A_4\cos[k\ (\sin\theta_2 + \sin\theta_4)y] \end{aligned} \tag{16}$$

As Eq. (16) suggested, the intensity distribution of the four-beam interference is equivalent to the two exposures of two-beam interference by rotating the substrate with 90°. When the incident angles are $\theta_1 = \theta_2 = \theta_3 = \theta_4 = \theta$, the periods in the x and y directions are $d_x = d_y = \lambda/2\sin\theta$. Fig. 7(b) shows the captured image of four-beam interference and the

measurements of phase shifts are illustrated in Fig. 7(c). The resulting periods in the x and y directions are 5.8121μm and 5.7192μm, respectively. According to Eq. (16), the incident angles can be concluded that $\theta_1 = \theta_3 = 3.17^\circ, and\ \theta_2 = \theta_4 = 3.12^\circ$ . With the help of theoretical and image analysis, the deviations of 93nm and $0.05^o$ have been determined.

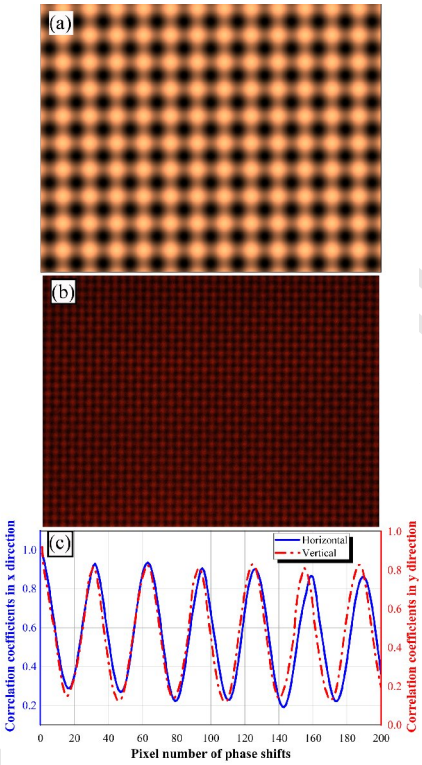


**Fig. 7** (a) 2D intensity profiles of the four-beam interference simulation; (b) The CCD image of the four-beam laser interference; (c) Corresponding correlation coefficients as a function of phase shifts.

*4.5 Potential applications*

It has been demonstrated that the proposed method is a powerful tool for analyzing almost all types of beam incidence conditions in LIL. Furthermore, the imaging system can also be integrated into an LIL system to achieve real-time imaging and lithography. The schematic of the innovative system is shown in Fig. 8. Additional beamsplitter mirrors or prisms are utilized to set up the imaging system, keeping the original optical path unchanged. Once the relationship of the incident angles between the LIL and imaging systems is

determined, real-time and dynamic calibrations can be achieved, which is an important application in LIL processes.

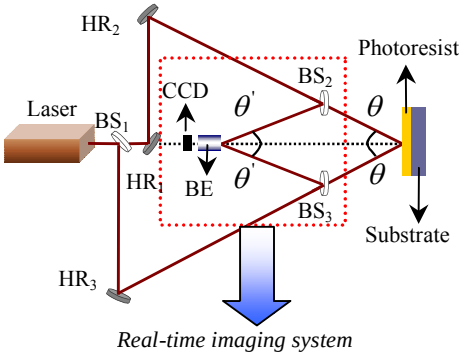


**Fig. 8** Schematic of the real-time imaging and lithography system.

## 5 Conclusions

In this work, beam incidence conditions are investigated theoretically and experimentally. It is demonstrated that beam incidence conditions have a significant impact on the period, contrast and formation of interference patterns. To determine the beam incidence conditions, the periods and contrasts of interference patterns are measured by means of image processing with subpixel accuracy and subsequently the incident angles and intensities of beams are calculated based on the theoretical analysis of spatial distributions of interfering beams. The relationship between the beam incidence conditions and interference patterns is revealed. The proposed method is useful for the control and calibration of LIL processes, and for reverse engineering applications.

**Acknowledgements**

This work was supported by National Key Basic Research Programs of China (973 Programs No.2012CB326406), National Natural Science Foundation Programs of China (No.61176002), Doctoral Programs of Higher Education of China (No.20112216110002), Jilin Provincial Science and Technology Programs (No.201115157 and No.20110704), Guangdong Science and Technology Programs (No.2009B091300006 and No.2011B010700101), Science and Technology Programs of Changchun City (No.09GH07

and No.11KP04), and Programs of Changchun University of Science and Technology (No.2013S001).

## References

1. Y. F. Liu, J. Feng, Y. G. Bai, J. F. Song, Y. Jin, Q. D. Chen, H. B. Sun, Omnidirectional emission from top-emitting organic light-emitting devices with microstructured cavity, Opt. Lett. 37 (2012) 124-126.
2. D. Wang, Z. Wang, Z. Zhang, Y. Yue, D. Li, C. Maple, Direct modification of silicon surface by nanosecond laser inteference lithography, Appl. Surf. Sci. 282 (2013) 67-72. .
3. D. Y. Xia, Z. Y. Ku, S. C. Lee, S. R. J. Brueck, Nanostructures and functional materials fabricated by interferometric lithography, Adv. Mater. 23 (2011) 147-179.
4. M. Ellman, A. Rodrıguez, N. Perez, M. Echeverria, Y. K. Verevkin, C. S. Peng, T. Berthou, Z. Wang, S. M. Olaizola, I. Ay-erdi, High-power laser interference lithography process on photoresist: Effect of laser fluence and polarisation, Appl. Surf. Sci. 255 (2008) 5537-5541.
5. A. Rodriguez, M. Echeverría, M. Ellman, N. Perez, Y. K. Verevkin, C. S. Peng, T. Berthou, Z. Wang, I. Ayerdi, J. Savall, S. M. Olaizola, Laser interference lithography for nanoscale structuring of materials: From laboratory to industry, Microelectron. Eng. 86 (2009) 929-936.
6. E. Ertorer, F. Vasefi, J. Keshwah, M. Najiminaini, C. Halfpap, U. Landbein, J. Carson, D. W. Hamilton, S. Mittler, Large area periodic, systematically changing, multishape nanostructures by laser interference lithography and cell response to these topographies, J. Biomed. Opt. 18 (2013) 035002.
7. L. Xu, L. S. Tan, M. H. Hong, Tuning of localized surface plasmon resonance of well-ordered Ag/Au bimetallic nanodot arrays by laser interference lithography and thermal annealing, Appl. Optics 50 (2011) G74-G79.
8. S. Qi, X. Yang, H. Lu, Research on multiple-beam interference of piontolite and measurement of minute wedge angle, Optik 124 (2013) 3586-3589.
9. L. Guo, H. B. Jiang, R. Q. Shao, Y. Zhang, S. Xie, J. Wang, X. Li, F. Jiang, Q. Chen, T. Zhang, H. B. Sun, Two-beam-laser interference mediated reduction, patterning and nanostructuring of graphene oxide for the production of a flexible humidity sensing device, Carbon 50 (2012) 1667-1673.
10. R. Guo, D. Yuan, S. Das, Large-area microlens arrays fabricated on flexible polycarbonate sheets via single-step laser interference ablation, J. Micromech. Microeng. 21 (2011) 150101-6.
11. Y. Jin, J. Feng, X. L. Zhang, M. Xu, Y. G. Bi, Q. D. Chen, H. Y. Wang, H. B. Sun, Surface plasmon enhanced absorption in organic solar cellsby employing a periodically corrugated metallic electrode, Appl.

Phys. Lett. 101 (2012) 1633031-3.

12. I. Castro-Hurtado, T. Tavera, P. Yurrita, N. Pérez, A. Rodriguez, G. G. Mandayo, E. Castaño, Structural and optical properties of WO3 sputtered thin films nanostructured by laser interference lithography, Appl. Surf. Sci. 276 (2013) 229-235.
13. D. Wu, Q. D. Chen, J. Yao, Y. C. Guan, J. N. Wang, L. G. Niu, H. H. Fang, H. B. Sun, A simple strategy to realize biomimetic surfaces with controlled anisotropic wetting, Appl. Phys. Lett. 96 (2010) 0537041-3.
14. D. Wang, Z. Wang, Z. Zhang, Y. Yue, D. Li, C. Maple, Modification of silicon surface by direct Laser interference, Proc. 3M-NANO, (2012) 5-8.
15. D. Wang, Z. Wang, Z. Zhang, Y. Yue, D. Li, C. Maple, Effects of polarization on four-beam laser interference lithography, Appl. Phys. Lett. 102 (2013) 0819031-5.
16. Z. Wang, C. Quan, P. J. Bryanston-Cross, Analysis of oblique fringes by fringe pattern matching, Proc. SPIE 4317 (2001) 160-165.
17. Z. Ji, J. Zhang, S. M. Olaizola, Y. K. Verevkin, C. Peng, C. Tan, T. Berthou, S. Tisserand, Z. Wang, Quality inspection of nanoscale patterns produced by laser interference lithography using image analysis techniques, Proc. IEEE ICMA (2009) 1835-1840.
18. X. Liu, L. Ma, H. Ren, B. Chen, L. Chai, W. Zheng, Multipe-surface interference fringes analysis basing on wavelength-modulated phase shifting interferometry, Optik 124 (2013) 4693-4696.
19. L. Liu, H. Pan, J. Xu, H. Xu, Y. Yue, D. Li, Z. Song, Z. Weng, Z. Hu, Z. Wang, J. Zhang, Oblique fringe measurement by pattern correlation, Proc. IEEE ICIA (2010) 940-945.
20. Z. Wang, S. Su, Y. K. Verevkin, S. Fatikow, Reference pattern-based 2D measurement with nano resolution, Proc. SPIE 6376 (2006) 63760M1-7.